Planetary Nebulae: An Eye to the Future
Proceedings IAU Symposium No. 283, 2011
A. Manchado, L. Stanghellini & D. Schönberner, eds.

doi:10.1017/S1743921312010630

Spitzer observations of planetary nebulae

You-Hua Chu

Department of Astronomy, University of Illinois,
1002 West Green Street, Urbana, Illinois, 61801, USA
email: yhchu@illinois.edu

Abstract. The Spitzer Space Telescope has three science instruments (IRAC, MIPS, and IRS) that can take images at 3.6, 4.5, 5.8, 8.0, 24, 70, and 160 μm, spectra over 5–38 μm, and spectral energy distribution over 52–100 μm. The Spitzer archive contains targeted imaging observations for more than 100 PNe. Spitzer legacy surveys, particularly the GLIMPSE survey of the Galactic plane, contain additional serendipitous imaging observations of PNe. Spitzer imaging and spectroscopic observations of PNe allow us to investigate atomic/molecular line emission and dust continuum from the nebulae as well as circumstellar dust disks around the central stars. Highlights of Spitzer observations of PNe are reviewed in this paper.

Keywords. Atomic processes, molecular processes, planetary nebulae: general, infrared: stars, surveys

1. Spitzer Space Telescope

The Spitzer Space Telescope (Werner *et al.* 2004), one of the four NASA's Great Observatories, is a 0.85 meter diameter, f/12 infrared (IR) telescope launched on August 25, 2003. It has an Earth-trailing heliocentric orbit so that the telescope is kept away from the Earth's heat and can be cooled more efficiently.

Spitzer has three science instruments:
(1) The Infrared Array Camera (IRAC; Fazio *et al.* 2004) has four detectors that take images at 3.6, 4.5, 5.8, and 8.0 μm, respectively.
(2) The Multiband Imaging Photometer for Spitzer (MIPS; Rieke *et al.* 2004) has three detector arrays for imaging at 24, 70, and 160 μm, respectively, and the 70 μm detector can also be used to measure spectral energy distributions (SEDs) from 52 to 100 μm at a spectral resolution of $\sim$7%.
(3) The InfraRed Spectrograph (IRS; Houck *et al.* 2004) has four modules that allow us to take spectra with a high ($\lambda/\Delta\lambda \sim 600$) or low ($\lambda/\Delta\lambda \sim 64$–$128$) resolution over the spectral range of 5–38 μm.
When the liquid helium coolant was exhausted, the "Warm Spitzer" phase started in May 2009, and only IRAC detectors at 3.6 and 4.5 μm remained useful.

Spitzer observations of PNe have been obtained by Guaranteed Time Observers (GTOs), Guest Observers (GOs), or legacy surveys of the Galactic plane and the Large and Small Magellanic Clouds (LMC & SMC). The GTOs are associated with the Spitzer instrument builders, and the GOs are open to the public. The surveys of the Galactic plane have been made for $l = \pm 65°$ and $b = \pm 1°$ in the four IRAC bands (GLIMPSE I and GLIMPSE II) and in MIPS 24 μm (MIPSGAL I and MIPSGAL II). The IRAC observations were extended to higher galactic latitudes for selected longitudes (GLIMPSE 3D) in all four bands, and extended to cover the rest of the Galactic plane in 3.6 and 4.5 μm during the Warm Spitzer mission (GLIMPSE360). A large number of PNe are expected to be covered by these GLIMPSE and MIPSGAL observations. The LMC and SMC were surveyed in all IRAC and MIPS bands (SAGE-LMC; SAGE-SMC; S^{3}MC).

Table 1. Spectral Features in the IRAC Bands

IRAC Band	PAH	HI Recom.	H_2 Rot.	Ion Forb.
3.6 μm	✓	✓		
4.5 μm		✓	✓	✓
5.8 μm	✓	✓	✓	✓
8.0 μm	✓	✓	✓	✓

All PNe, except the outlying members, in the LMC and SMC were included in these surveys.

2. IRAC Observations of PNe

The four IRAC bands contain different combinations of polycyclic aromatic hydrocarbon (PAH) features, HI recombination lines, H_2 rotational transitions, and forbidden lines of atoms/ions, as marked in Table 1 and seen in the ISO spectra of NGC 7027 (Bernard-Salas *et al.* 2001) and Hb 12 (Hora *et al.* 2004). To interpret IRAC images, spectra or images at other wavelengths are needed. Nevertheless, IRAC images often reveal morphological features that bear implications on PN formation mechanisms but are less well seen in other wavelengths. These features include: (1) Molecular knots – the Helix Nebula is the best example and the molecular nature of its knots has been confirmed spectroscopically by Hora *et al.* (2006); IRAC 8 μm images of A21 and JnEr 1 in Figure 1 also show molecular knots. (2) Large halos – IRAC 8 μm images frequently show prominent, extended halos similar to those seen in optical emission lines (Corradi *et al.* 2003); six new halos are shown in Figure 2. (3) Concentric rings – IRAC images of PNe also reveal concentric rings similar to those seen in optical emission lines (Corradi *et al.* 2004); two examples are shown in Figure 3. (4) Circular rings in halos – IRAC 8 μm images of NGC 6072 and NGC 6720 in Figure 3 show an almost perfectly circular ring in the halo that is not obvious in optical images. (5) PAH emission peaks of ionization bounded nebulae – PAH emission can peak in the photodissociation regions (PDRs) around the photoionized PN, for example, NGC 2610 in Figure 4.

Since the initial report of IRAC observations of PNe (Hora *et al.* 2004), not many analyses of spatially-resolved IRAC images of PNe have been published. A detailed analysis of IRAC images of the Helix Nebula complemented by spectroscopic observations was carried out by Hora *et al.* (2006). Phillips & Ramos-Larios (2008a) analyzed quantitatively IRAC images of 18 PNe and suggest that PAH emission from PDRs contributes significantly to the observed mid-IR fluxes. Phillips & Ramos-Larios (2010) extended their analysis to seven bipolar PNe, assessing the roles of PAH emission from PDRs and shock excited H_2 emission, and discussing the color variations from the cores to the lobes. Cerrigone *et al.* (2008) analyzed IRAC images, in conjunction with 4.8 and 8.6 GHz radio continuum observations, of the bipolar PN IC 4406, and concluded that there exist at least three dust components at temperatures ranging from 57 to 700 K.

The GLIMPSE surveys have been used to search for new PNe. Phillips & Ramos-Larios (2008b) found 12 new and possible PNe in GLIMPSE I. Kwok *et al.* (2008) also used GLIMPSE I survey data to search for new PNe; however, about 1/3 of the 30 PNe they suggested are likely HII regions in the Galactic plane. Zhang & Kwok (2009) used GLIMPSE II, complemented by MIPS 24 μm and Hα images, to identify 37 new PNe. Finally, Quino-Mendoza *et al.* (2011) have used the GLIMPSE3D survey to make quantitative analyses of the color and surface brightness variations in 24 PNe.

https://doi.org/10.1017/S1743921312010630 Published online by Cambridge University Press

IRAC observations of PNe have been used to investigate how their IR colors can be used to identify new PNe. Using different combinations of IRAC bands, such as [3.6]−[4.5], [4.5]−[8.0], and [5.8]−[8.0], color-color diagrams have been constructed for 12 Galactic PNe (Hora *et al.* 2004), 233 PNe in the LMC (Hora *et al.* 2008), 58 PNe from the MASH sample (Cohen *et al.* 2007), 136 PNe in the GLIMPSE I survey (Cohen *et al.* 2011), and 367 PNe from the Galaxy and the LMC (Phillips & Ramos-Larios 2009). As shown in the left panel of Figure 5 and concluded by Hora *et al.* (2008) and Gruendl & Chu (2009), PNe are well separated from stars in color-color and color-magnitude diagrams, but overlap significantly with young stellar objects and background galaxies. To unambiguously identify PNe, morphological information of the nebulae and their environments and/or spectra are still needed. An interesting color evolution, shown in the right panels of Figure 5, has been noted by Cohen *et al.* (2011); the IRAC 5.8 μm band flux increases with PN size and it is attributed to an increasing contribution from the 6.2 μm PAH band emission as PNe age.

3. MIPS Observations of PNe

The three MIPS bands, 24, 70, and 160 μm, are ideal for investigation of dust continuum emission; however, their point-spread functions, FWHM 6″, 18″, and 40″, respectively, severely limit the number of PNe that are adequately resolved in the 70 and 160 μm bands for detailed analysis. Spatially resolved analyses of PNe utilizing all MIPS bands have been reported for only two bipolar nebulae, NGC 2346 and NGC 650. For NGC 2346, Su *et al.* (2004) show that the 24 μm image exhibits a bipolar morphology resembling that seen in the optical [N II] image, the 70 μm emission is concentrated in a torus where the bipolar lobes join, and the 160 μm emission is much more extended and showing spherical symmetry. They suggest that the mass loss changed from spherical symmetric to non-spherical due to the binary central star of NGC 2346. For NGC 650, Ueta (2006) finds the 24 μm image similar to the [O III] image and suggests that the [O IV] 25.89 μm line emission dominates the MIPS 24 μm band flux; he finds the 70 and

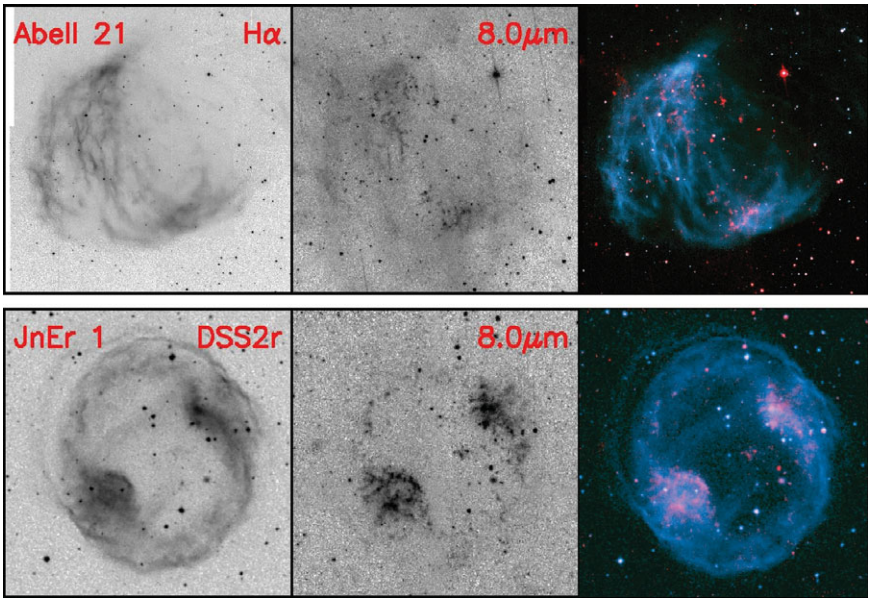

Figure 1. Images of PNe A21 and JnEr 1 illustrating molecular knots.

https://doi.org/10.1017/S1743921312010630 Published online by Cambridge University Press

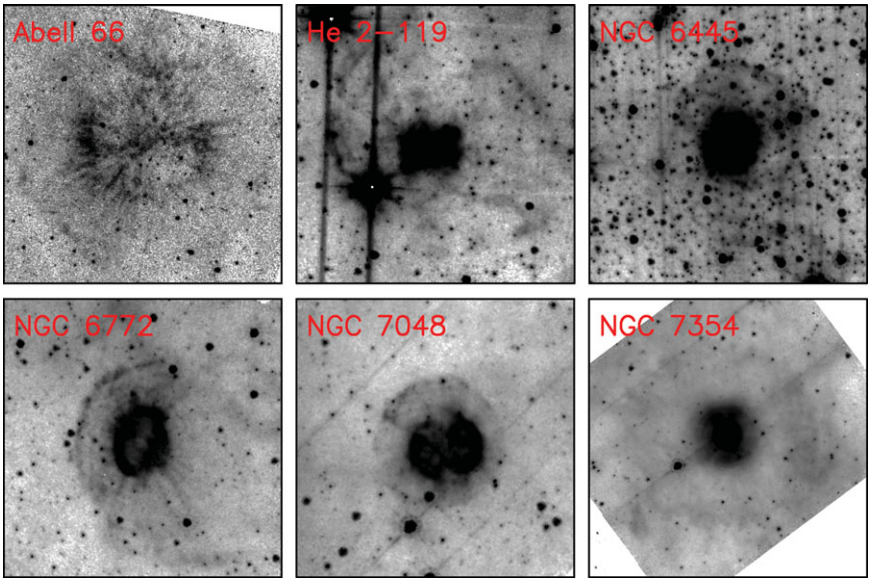

Figure 2. IRAC 8 μm images of PNe A66, He 2-119, NGC 6445, NGC 6772, NGC 7048, and NGC 7354 showing large halos.

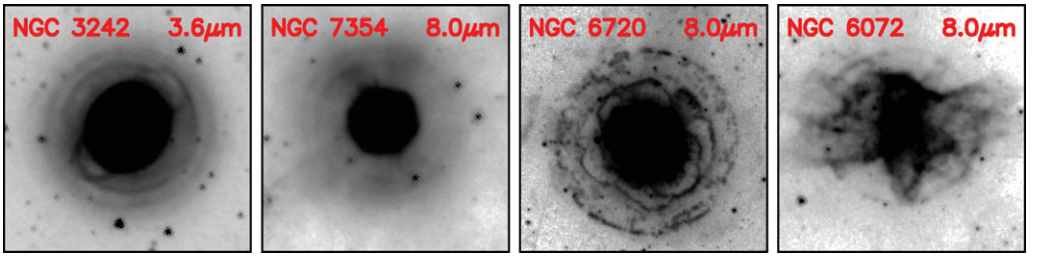

Figure 3. IRAC 3.6 μm image of NGC 3242 and 8.0 μm image of NGC 7354 showing concentric rings, and IRAC 8.0 μm images of NGC 6720 and NGC 6072 showing an almost perfectly circular ring in the halo.

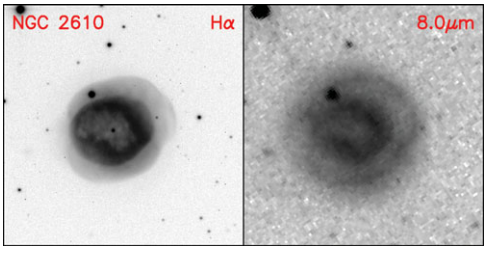

Figure 4. Hα and IRAC 8.0 μm images of NGC 2610 showing the PAH emission along the outer rim.

160 μm emission in the torus/waist more extended than the 24 μm emission and suggests that mass loss was mainly in the equatorial, rather than polar, directions.

MIPS 24 μm images of PNe are useful in revealing regions of high ionization as well as dust emission. The MIPS 24 μm band includes high-ionization [O IV] 25.89 μm and [Ne V] 24.3 μm lines and dust continuum that are frequently seen in PNe. Large numbers of MIPS 24 μm observations of PNe have been reported by Phillips & Marguez-Lugo (2011)

https://doi.org/10.1017/S1743921312010630 Published online by Cambridge University Press

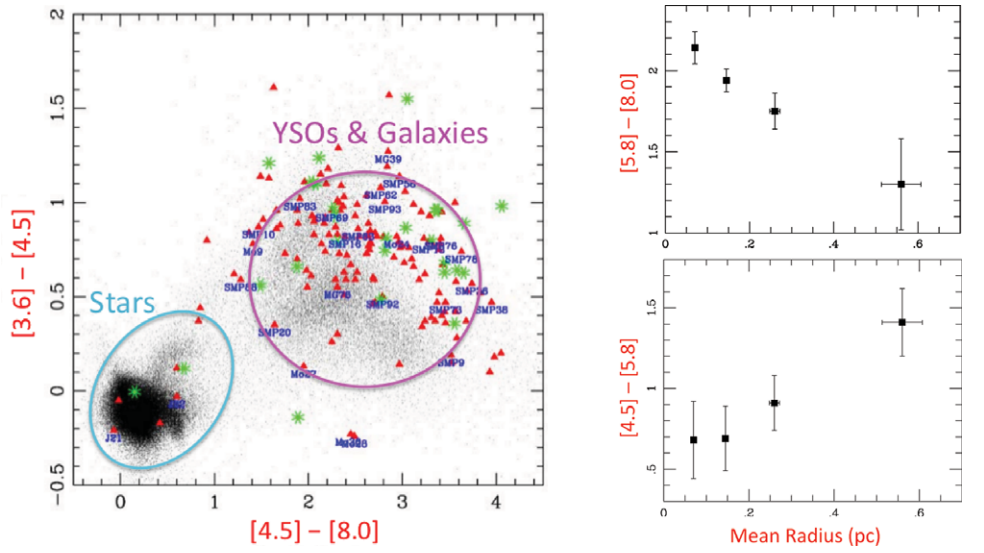

Figure 5. Left:Color-color diagram of sources in the LMC (Hora *et al.* 2008). The triangles mark known PNe in the LMC, and asterisks Galactic PNe. The ellipse at the lower left encloses locations of stars, and the upper ellipse encloses the general locations of young stellar objects (YSOs) and background galaxies. **Right**: Color-size plots of PNe from GLIMPSE I (Cohen *et al.* 2011).

and Chu *et al.* (2009). The former investigation used the MIPSGAL data (each ∼30 s exposure) to analyze 224 PNe in the Galactic plane, comparing the 24 μm profiles to IRAC profiles and constructing color-color diagrams. The latter obtained 24 μm images for 36 PNe each with 420 s exposure, compared the 24 μm profiles to Hα profiles, and obtained IRS spectra to probe the nature of the 24 μm emission.

Hα emission is an excellent tracer for dense ionized gas. Comparing 24 μm and Hα profiles, Chu *et al.* (2009) find three types of correspondences, as illustrated in Figure 6: (1) 24 μm emission more extended than Hα emission – as the [O IV] and [Ne V] lines originate from high-ionization regions, the 24 μm emission from the outer parts of PNe must be dominated by dust continuum; (2) similar morphology and spatial extent between 24 μm and Hα – both line emission and dust continuum can contribute to the 24 μm band flux; (3) 24 μm emission at center of Hα shell – low densities and high excitation are expected in central regions of PNe, and thus the 24 μm emission must be dominated by [O IV] and some [Ne V] line emission. IRS spectrum of the diffuse 24 μm emission in the central region of Sh 2-188 shows that the emission is indeed dominated by the [O IV] 25.89 μm emission (Chu *et al.* 2009).

4. IRS Observations of PNe

A picture is worth a thousand words, while a spectrum is worth a thousand pictures. The most exciting Spitzer results of PNe are derived from IRS observations, which have many advantages over spectroscopic observations in optical wavelengths for studies of abundances of ionized gas, exciting/fundamental molecules, and dust properties.

IRS studies of abundances of ionized gas in PNe have the following advantages: (1) extinction has little effects at mid-IR wavelengths; (2) mid-IR transitions are close to the ground level and thus insensitive to the temperature; (3) most ionization stages of Ne, S, and Ar are covered and thus there is no need to resort to ionization correction

https://doi.org/10.1017/S1743921312010630 Published online by Cambridge University Press

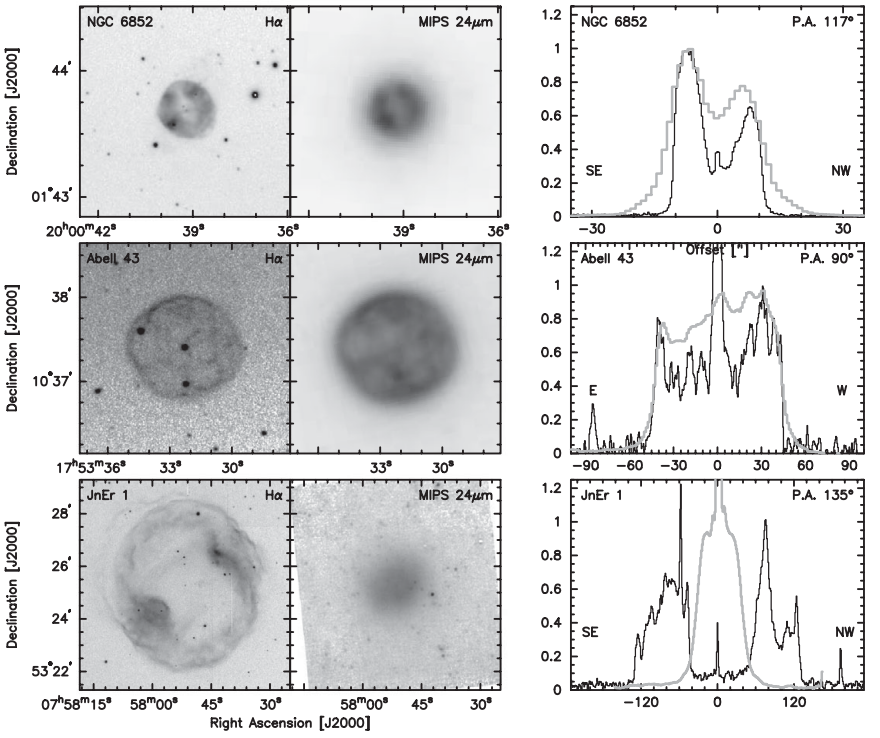

Figure 6. Hα and 24 μm images of NGC 6852, A43, and JnEr 1. The right panels compare the Hα (dark) and 24 μm (grey) surface brightness profiles. Taken from Chu *et al.* (2009).

factors; and (4) [Fe III] 22.93 μm, [Fe II] 17.94 μm, [Cl IV] 20.32 and 11.76 μm, and [P III] 17.89 μm lines allow determinations of Fe, Cl, and P abundances.

Therefore, many Galactic PNe have been observed for abundance analyses, and the nebular abundances are further compared to models of stellar evolution and nucleosynthesis to determine the mass of progenitor stars: IC 2448, M 1-42, NGC 2392, NGC 2792, NGC 3242, NGC 6210, NGC 6369 (Guiles *et al.* 2007; Pottasch *et al.* 2008, 2009a, 2009b; Pottasch & Bernard-Salas 2008). Abundances of the halo PN DdDm-1 have been analyzed by Henry *et al.* (2008) and the most O-deficient PN TS01 by Stasińska *et al.* (2010). See Kwitter (this volume) for a review of PN abundances.

Bernard-Salas *et al.* (2004) analyzed the abundances of the LMC PN SMP 83. Bernard-Salas *et al.* (2008) analyzed Ne and S abundances for 25 PNe in the LMC and SMC, finding LMC and SMC Ne abundances to be $\sim$1/3 and 1/6 of the Galactic values, respectively; furthermore, the Ne/S ratio is higher in the MC PNe, $\sim$23.5, than in the Galactic PNe, $\sim$16. Shaw *et al.* (2010) analyzed elemental abundances of He, N, O, Ne, S, and Ar for 14 PNe in the SMC, and found that ionization correction factors work well even in low-metalicity conditions, except for PNe with very high ionization.

The most exciting discovery in PNe made by IRS observations is the detection of fullerenes. C_{60} and C_{70} were produced in laboratory more than 25 years ago (Kroto *et al.* 1985), and they might be responsible for the diffuse interstellar bands and provide catalyst for prebiotic chemistry. However, they have not been unambiguously detected until IRS observations of PNe were made (Figure 7). Cami *et al.* (2010) reported the first detection of C_{60} and C_{70} in the PN TC 1, and suggested that fullerenes can be produced only in H-deficient environments. However, this suggestion has been challenged by

https://doi.org/10.1017/S1743921312010630 Published online by Cambridge University Press

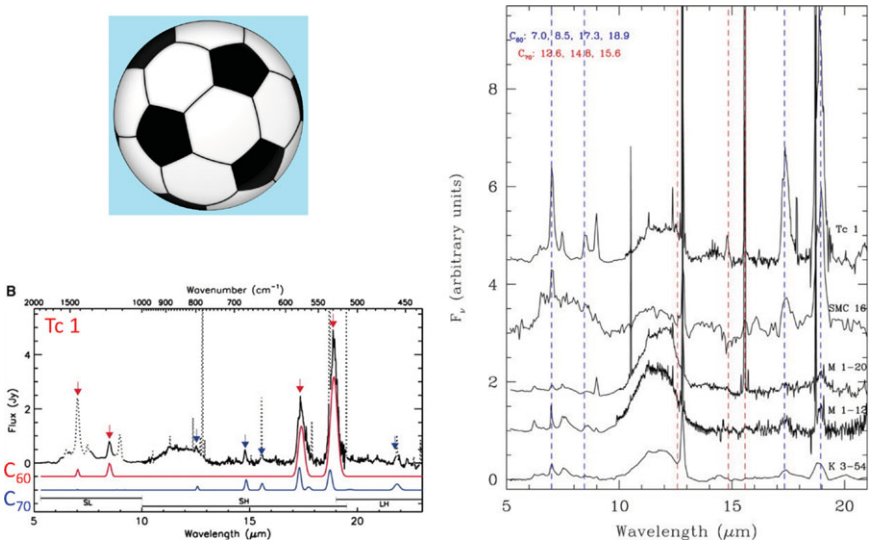

Figure 7. Spectra of fullerene in PNe. The left panel is from Cami *et al.* (2010) and the right panel from García-Hernández *et al.* (2010).

García-Hernández *et al.* (2010), who detected fullerene in H-containing PNe in the Galaxy and in the SMC. The simultaneous presence of PAHs and fullerenes is suggestive that they may both be formed by photochemical processing of hydrogenated amorphous carbons.

IRS spectra of 11 PNe in the Galactic bulge have been studied by Gutenkunst *et al.* (2008) – these spectra are dominated by O-rich dust features (crystalline silicates) that are rare in disk PNe; furthermore, roughly 1/2 of these bulge PNe also show C-rich dust features (PAHs), i.e., dual chemistry. They suggest that the dual chemistry is caused by binary evolution, with the PAHs located in the current outflow and the crystalline silicates in an old disk created by binary interaction. This mixed chemistry phenomenon in Galactic bulge PNe was re-examined by Perea-Calderón *et al.* (2009), who analyzed 40 Galactic PNe of which 26 belong to the bulge. These authors propose a different explanation for the dual chemistry – the final thermal pulse of the AGB produced enhanced mass loss, removing the remaining H-rich envelope, exposing the C-rich layer, and generating shocks to produce the crystalline silicates.

Stanghellini *et al.* (2007; this volume) made IRS observations of a large number of PNe in the LMC and the SMC. These observations will be complemented by images and long-slit spectra obtained with the Hubble Space Telescope as well as ground-based telescopes. As the distances to these PNe are well known, it is possible to analyze dust properties of these PNe and compare them with the evolutionary status of their central stars for the most comprehensive picture.

5. Spitzer Observations of CSPNs

Spitzer MIPS observations of the Helix Nebula show a bright unresolved source coincident with the central star in both the 24 and 70 μm bands. Followup IRS observations confirm the dust continuum nature of this excess mid-IR emission. The color temperature of the IR emitter is 90-130 K, too cold to be a star. The IR luminosity requires an emitting area of 4-40 AU^2, which can be provided only by a dust disk. For a stellar temperature of ∼110,000 K, the dust disk must be 35-150 AU from the central star. As such a distance corresponds to the Kuiper Belt in the Solar System, Su *et al.* (2007) suggest that the dusk disk is produced by collisions among Kuiper Belt-like objects.

https://doi.org/10.1017/S1743921312010630 Published online by Cambridge University Press

To search for dust disks similar to that of the Helix central star, Chu *et al.* (2011) made a MIPS 24 μm survey of 71 hot white dwarfs, about 1/2 of which are still in PNe. They find 24 μm excesses in 9 objects, among which 7 are in PNe. Inspired by the prevalence of IR excesses in central stars of PNe, Bilikova *et al.* (this volume) made an Spitzer archival search for IR excesses of PN central stars and made followup spectroscopic observations using Spitzer IRS and Gemini NIRI and Michelle. While spectroscopic observations show that most of the IR excesses are dominated by dust continuum, some also show emission lines or even silicate features. These dust disks may have resulted from planetary disk evolution or binary central star interactions.

References

Bernard Salas, J., Pottasch, S. R., Beintema, D. A., & Wesselius, P. R. 2001, *A&A*, 367, 949
Bernard-Salas, J., Houck, J. R., Morris, P. W., *et al.* 2004, *ApJS*, 154, 271
Bernard-Salas, J., Pottasch, S. R., Gutenkunst, S., *et al.* 2008, *ApJ*, 672, 274
Cami, J., Bernard-Salas, J., Peeters, E., & Malek, S. E. 2010, *Science*, 329, 1180
Cerrigone, L., Hora, J. L., Umana, G., & Trigilio, C. 2008, *ApJ*, 682, 1047
Chu, Y.-H., Gruendl, R. A., Guerrero, M. A., *et al.* 2009, *AJ*, 138, 691
Chu, Y.-H., Su, K. Y. L., Bilikova, J., *et al.* 2011, *AJ*, 142, 75
Cohen, M., Parker, Q. A., Green, A. J., *et al.* 2007, *ApJ*, 669, 343
Cohen, M., Parker, Q. A., Green, A. J., *et al.* 2011, *MNRAS*, 413, 514
Corradi, R. L. M., Sánchez-Blázquez, P., Mellema, G., *et al.* 2004, *A&A*, 417, 637
Corradi, R. L. M., Schönberner, D., Steffen, M., & Perinotto, M. 2003, *MNRAS*, 340, 417
Fazio, G. G., Hora, J. L., Allen, L. E., *et al.* 2004, *ApJS*, 154, 10
García-Hernández, D. A., Manchado, A., García-Lario, P., *et al.* 2010, *ApJL*, 724, L39
Gruendl, R. A. & Chu, Y.-H. 2009, *ApJS*, 184, 172
Guiles, S., Bernard-Salas, J., Pottasch, S. R., & Roellig, T. L. 2007, *ApJ*, 660, 1282
Gutenkunst, S., Bernard-Salas, J., Pottasch, S. R., *et al.* 2008, *ApJ*, 680, 1206
Henry, R. B. C.., Kwitter, K. B., Dufour, R. J., & Skinner, J. N. 2008, *ApJ*, 680, 1162
Hora, J. L., Cohen, M., Ellis, R. G., *et al.* 2008, *AJ*, 135, 726
Hora, J.L., Latter, W.B., Allen, L.E., *et al.* 2004 *ApJS*, 154, 296
Hora, J. L., Latter, W. B., Smith, H. A., & Marengo, M. 2006, *ApJ*, 652, 426
Houck, J. R., Roellig, T. L., van Cleve, J., *et al.* 2004, *ApJS*, 154, 18
Kroto, H. W., Heath, J. R., Obrien, S. C., Curl, R. F., & Smalley, R. E. 1985, *Nature*, 318, 162
Kwok, S., Zhang, Y., Koning, N., Huang, H.-H., & Churchwell, E. 2008, *ApJS*, 174, 426
Perea-Calderón, J. V., García-Hernández, D. A., García-Lario, P., *et al.* 2009, *A&AL*, 495, L5
Phillips, J. P. & Marquez-Lugo, R. A. 2011, *MNRAS*, 410, 2257
Phillips, J. P. & Ramos-Larios, G. 2008a, *MNRAS*, 383, 1029
Phillips, J. P. & Ramos-Larios, G. 2008b, *MNRAS*, 386, 995
Phillips, J. P. & Ramos-Larios, G. 2009, *MNRAS*, 396, 1915
Phillips, J. P. & Ramos-Larios, G. 2010, *MNRAS*, 405, 2179
Pottasch, S. R. & Bernard-Salas, J. 2008, *A&A*, 490, 715
Pottasch, S. R., Bernard-Salas, J., & Roellig, T. L. 2008, *A&A*, 481, 393
Pottasch, S. R., Bernard-Salas, J., & Roellig, T. L. 2009a, *A&A*, 499, 249
Pottasch, S. R., Surendiranath, R., Bernard-Salas, J., & Roellig, T. L. 2009b, *A&A*, 502, 189
Quino-Mendoza, J. A., Phillips, J. P., & Ramos-Larios, G. 2011, *RMxAA*, 47, 31
Rieke, G. H., Young, E. T., Engelbracht, C. W., *et al.* 2004, *ApJS*, 154, 25
Shaw, R. A., Lee, T.-H., Stanghellini, L., *et al.* 2010, *ApJ*, 717, 562
Stanghellini, L., García-Lario, P., García-Hernández, D. A., *et al.* 2007, *ApJ*, 671, 1669
Stasińska, G., Morisset, C., Tovmassian, G., *et al.* 2010, *A&A*, 511, A44
Su, K. Y. L., Chu, Y.-H., Rieke, G. H., *et al.* 2007, *ApJL*, 28, 490
Su, K. Y. L., Kelly, D. M., Latter, W. B., *et al.* 2004, *ApJS*, 154, 302
Ueta, T. 2006, *ApJ*, 650, 228
Werner, M. W., Roellig, T. L., Low, F. J., *et al.* 2004, *ApJS*, 154, 1
Zhang, Y. & Kwok, S. 2009, *ApJ*, 706, 252